PERGAMON

Journal of Structural Geology 22 (2000) 627–645

JOURNAL OF STRUCTURAL GEOLOGY

www.elsevier.nl/locate/jstrugeo

Cenozoic folding and faulting in the south Aquitaine Basin (France): insights from combined structural and paleostress analyses

Muriel Rocher[a], Olivier Lacombe[a,*], Jacques Angelier[a], Benoît Deffontaines[a], François Verdier[b]

[a]*Université P. & M. Curie, ESA 7072, CNRS, Laboratoire de Tectonique Quantitative, Tr 25-26, E1, Boîte 129, 4 place Jussieu, 75252 Paris Cedex 05, France*

[b]*Gaz de France, Direction de la Recherche, Département Réservoirs Souterrains, La Plaine Saint Denis, France*

Received 22 April 1998; accepted 23 November 1999

Abstract

New fieldwork, surface data (e.g. drainage network anomalies) and SPOT satellite imagery are combined with sub-surface data (seismic profiles and drill-cores) to analyse the structural setting of the south Aquitaine Basin. Cenozoic paleostresses are determined through inversion of fault slip and calcite twin data (quarries and drill cores), allowing reconstruction of the Cenozoic structural and tectonic evolution. The main tectonic event, the NNE 'Pyrenean compression', from the Late Cretaceous to the Oligocene, is responsible for thrusting and folding along N110° axes and strike-slip reactivation of major NNW and NE–SW faults. Some fold axes turn along NNW major wrench faults, and compression locally undergoes deviation to ENE trends. NNE extension locally occurred at anticline hinges. After a minor WNW extension, a Miocene NNW compression occurred and changed into a perpendicular ENE extension, responsible for nearly N–S normal faulting.

These multiple states of stress reflect two major compressional events (NNE and NNW); their variety mainly reveals local accommodation due to numerous inherited structures, in the general context of Eurasia–Africa convergence.

1. Structural setting and scope of the study

The structure of the South-Aquitaine Basin (northwestern Pyrenean foreland, France) is dominated by N110-trending folds and thrusts (Fig. 1a), which formed during the so-called 'Pyrenean tectonic phase', consequent to the N–S convergence of Africa and Eurasia plates. Most anticlines correspond to north-vergent fault-propagation folds, striking parallel to the Pyrenean Belt. Following Mesozoic extensions (see below), this Cenozoic tectogenesis was dominated by nearly N–S compression, which prevailed from the Late Cretaceous to the Oligocene. The progressive northward migration of the foreland Pyrenean flexure accompanied the setting of the Pyrenean thrust units, successively incorporating and deforming foredeep sediments (Déramond et al., 1993).

The structure of the Aquitaine Basin is mainly inherited from the Late Carboniferous Variscan orogeny, and from Mesozoic extensions, including Triassic basin formation, Jurassic extension and Middle Cretaceous dislocation of the Aquitaine Platform.

During the Late Paleozoic, the Variscan orogeny generated the Variscan Belt in Central France with folding trending N110. Accordingly, N050–070 and N030 sinistral and N150 dextral faults developed in the Aquitaine basement (Debelmas, 1986; Lefort, 1989).

The NNE-trending extension (read: NNE–SSW) re-

* Corresponding author.
E-mail address: olivier.lacombe@lgs.jussieu.fr (O. Lacombe).

0191-8141/00/$ - see front matter
PII: S0191-8141(99)00181-9

sponsible for the formation of the Aquitaine Basin appeared as early as the Permian (Winnock, 1974; Boillot, 1984; Autran and Cogné, 1980). The Arzacq and northern sub-basins (forming the Aquitaine Basin) began to develop in response to a high rate of tensional subsidence, each one being split into several second-order basins by N160 sinistral faults. The pianokey type differential tilting along such fault lines delimit future major paleogeographic domains. In the Arzacq basin, Triassic formations (sandstones, evaporites and clays) become thinner toward the north and the east (Winnock, 1974). This Late Paleozoic–Early Mesozoic structural pattern had important consequences for the forthcoming Pyrenean deformation: décollement of the cover occurred in the western part of the Aquitaine Basin where Triassic deposits were thick (that is above the Triassic paleo-basins).

During the Late Jurassic, the extension was trending nearly NE–SW, with WNW normal faults and NE–SW transfer faults. The first migration of Triassic salts occurred along the WNW ridges, as, for example, the Audignon anticline (Fig. 1) (Stévaux and Zolnaï, 1975).

From Barremian to Albian, a NW-trending extension was associated with the paroxysmal dislocation of the Aquitaine Basin (Brunet, 1991). The Iberia–Eurasia boundary underwent a left-lateral movement associated with the opening of the North Atlantic

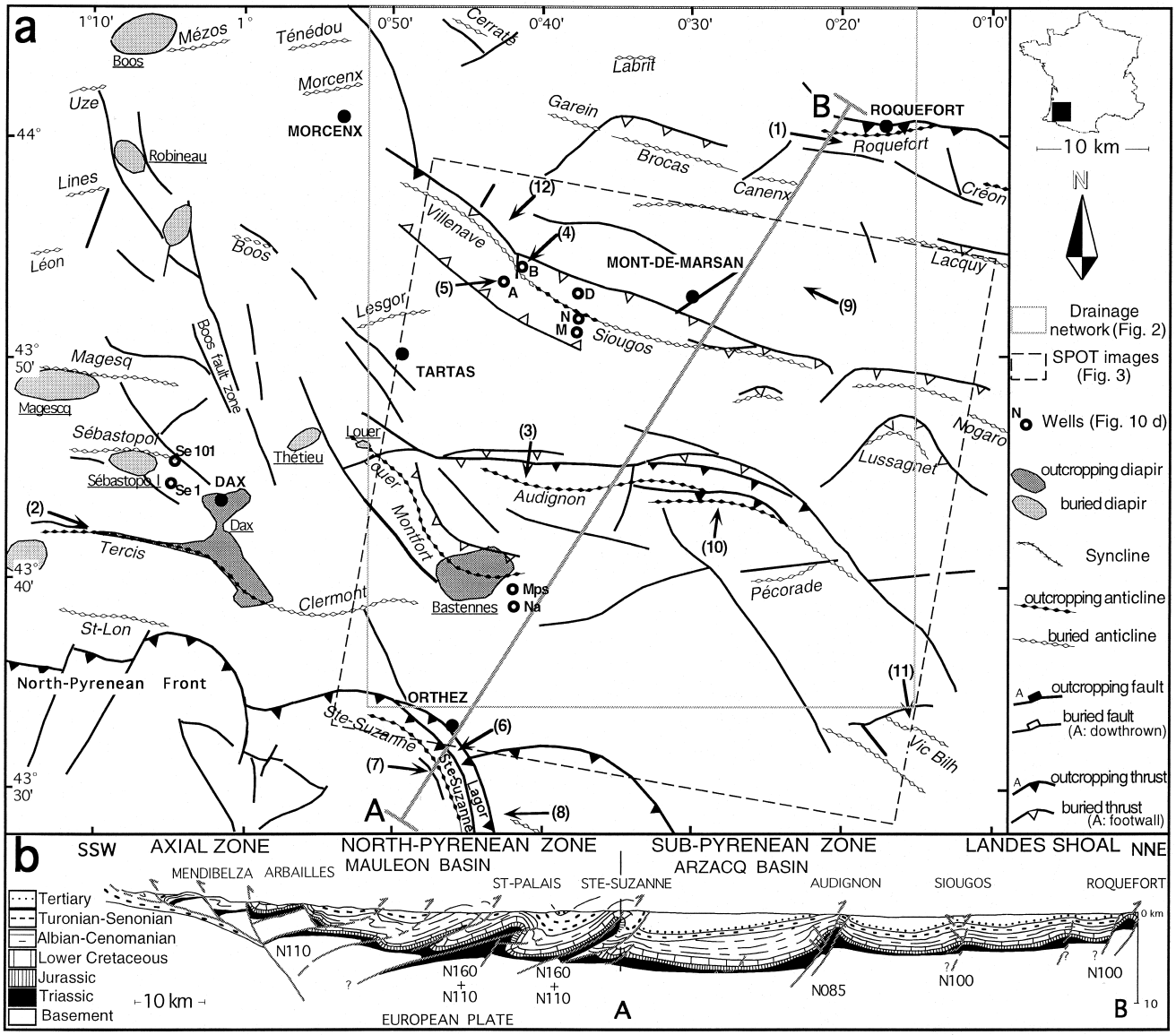

Fig. 1. (a) General structural sketch map of the studied area. Tectonic sites are situated on each arrowhead and numbered: (1) Cros, (2) Tercis, (3): Arcet, (4) and (5) respectively, wells A and B of Siougos, (6) La Ménière, (7) Sainte-Suzanne, (8) Loubieng, (9) Bougue, (10) Sarraziet, (11) Vic-Bilh, (12) Vivès. (b) Geological cross-section deduced from ECORS-Arzacq line (ECORS Pyrenees team, 1988) elongated to the Landes.

Ocean, the Bay of Biscay, and the Parentis basin (Mid-Aptian). This left-lateral movement resulted in the development of pull-apart basins associated with N140-trending sinistral faults and N060-trending normal faults (Brunet, 1991). Then, from Albian to Late Cretaceous, the N110 faults underwent a sinistral movement.

Finally, during the uppermost Cretaceous and Cenozoic, in the Aquitaine basin, Mesozoic NNW- and NE–SW-trending faults were reactivated as strike-slip faults along which evaporites migrated, and fold–thrust systems developed parallel to the N100–N110 Variscan Belt.

In this paper, we focus on the development of the northernmost structures of the Pyrenean belt. Recent studies showed that the present-day stress remains dominated by nearly N–S compression. However, the stress field is either perturbed (e.g. $\sigma_1 - \sigma_2$ permutations) or has deviated close to major inherited structural features (Bell et al., 1992). By means of paleostress reconstructions, we aim to evaluate how long the Pyrenean compression prevailed, and how much it was influenced by possible kinematic changes. This implies a focus on the nature, extent and origin of paleostress perturbations. The scope of this study is to provide new insights on the structural evolution of the Aquitaine Basin since the beginning of the Pyrenean collision, with emphasis on the relationships between major structures and paleostress orientations.

To fulfil these requirements, a thorough reconstruction of tectonic paleostress patterns was indispensable. In the region of Mont-de-Marsan, because pre-Miocene natural scarps are few, we analysed tectonic features, such as striated faults and calcite twins, in both quarries and drill-cores. For a better understanding of the relationships between paleostresses, wrench faults and fold–thrust systems, we additionally investigated an exposed anticline genetically similar to the commonly buried structures—the Sainte-Suzanne anticline—located along the North Pyrenean Front (Fig. 1).

2. Structural analysis from sub-surface and surface data

Because most tectonic features are buried beneath post-collisional Miocene to Quaternary deposits, our structural analysis combined fieldwork, surface investigations from analyses of drainage pattern anomalies and SPOT satellite imagery, with subsurface data, including seismic reflection profiles and information from drill-cores. This allowed us to improve the regional structural geology map. However, the continuity between major fault segments was difficult to establish from sparse field observations, so that a thorough mapping of the deformation field could not be done. It is known that the minor fault patterns usually reflect the regional tectonic style, so we use this opportunity to reconstruct tectonic mechanisms. Provided that local stress perturbations can be identified, the analysis of minor fracture patterns thus constitutes a powerful tool to reconstruct the far-field paleostresses (see Section 3).

Such a multisource analysis brings strong constraints on both the regional structural evolution through time and the kinematics of the major faults, even though they are presently hidden by overlying sediments. As an example, a single regional compressional strike-slip state of stress accounts for the development of most folds, reverse and strike-slip faults and tension gashes, although these features are in fact observable in very few outcrops. As a result, paleostress reconstructions lead to more regionally significant information than that provided by the sole local observation of deformation.

2.1. Drainage pattern anomalies

In the flat Aquitaine region where scarps are scarce, the analysis of the hydrographic network is a useful tool for structural mapping. It is known that studies of drainage patterns bring significant contribution to structural analyses (e.g. Deffontaines and Chorowicz, 1991), even where structures are buried (Scanvic, 1983). The development of the drainage network is influenced by external factors (e.g. climate, forest, agricultural practice), internal factors (e.g. lithology, dip-slope, diapirs, folds and faults), and composite factors (e.g. eustatic changes).

In Fig. 2(a), we transferred the drainage network extracted from the I.G.N. 1/25 000 topographic maps of the Landes region, supplemented with temporary water courses and backwater deduced from topography, from which we extracted rectilinear and curvilinear drainage pattern anomalies. Anticlines and synclines generate a particular network (Deffontaines, 1990), including annular drainage and curvilinear anomalies on their termination; faulting and lithology generate rectilinear drainage anomalies.

Drainage anomalies occur along various directions: N–S, N040, E–W, N120 and N160 (Fig. 2b). Because bedding planes are frequently trending nearly N110, parallel to the anticline axes, it is difficult to discriminate the E–W to N120 waterways following beds from those following faults.

Three regions called A, B and C, separated by evaporitic ridges called 'Celtaquitaine flexure' CF (Labrit, Roquefort, Créon, Barbotan anticlines) and 'Gasconne flexure' GF (Tercis, Montfort, Audignon anticlines), are shown on Fig. 2. In the A region, major structures trend E–W to N120 (strata limits, folds and thrusts); few rectilinear anomalies trend N–S. The B region dis-

plays N040 rectilinear anomalies (like that near Tartas), some N–S anomalies (e.g. guiding of the Adour River, arrow Fig. 2) and few N140 and E–W anomalies. The C region is bounded on the NE and the SW by NNW fault zones. Some N–S, N040 and E–W anomalies are also identified. Numerous curvilinear anomalies exist near the Bastennes diapir structure (BD).

A limit of this surface investigation is imposed by the local scarceness of the drainage network, as in A and B areas (Fig. 2a). It is thus difficult to recognize the tectonic structures in these zones. Satellite imagery provides additional information on subsurface structures.

2.2. SPOT satellite images

Panchromatic SPOT images are in the visible band of wavelength, from 0.51 to 0.73 μm. Their major advantage is the accuracy, with 10-m ground resolution. We used two scenes approximately in the same area (KJ: 38-261). The region covered by each image is 60×60 km in size (Fig. 1a).

SPOT analysis in a temperate area is limited by dense groundcover in the NW, and intense agricultural activity, complicating the interpretation. However, these images allowed an accurate location of folds and major faults, especially taking into account flanks, plateau and crest morphologies (Fig. 3). Fault types have been identified from visible offsets (folds, other faults, bedding) and from the dip of the fault planes. These images thus provided limited, but useful information on both the geometry and the kinematics of regional structures.

As for drainage network studies, we divided the region into A, B and C areas. The crescent-shaped Audignon anticline separates B and C regions (Fig. 3). In the B region (Armagnac basin), we observe N110-trending folds associated with parallel thrusts. Few NNW dextral faults and N–S faults occur. Some

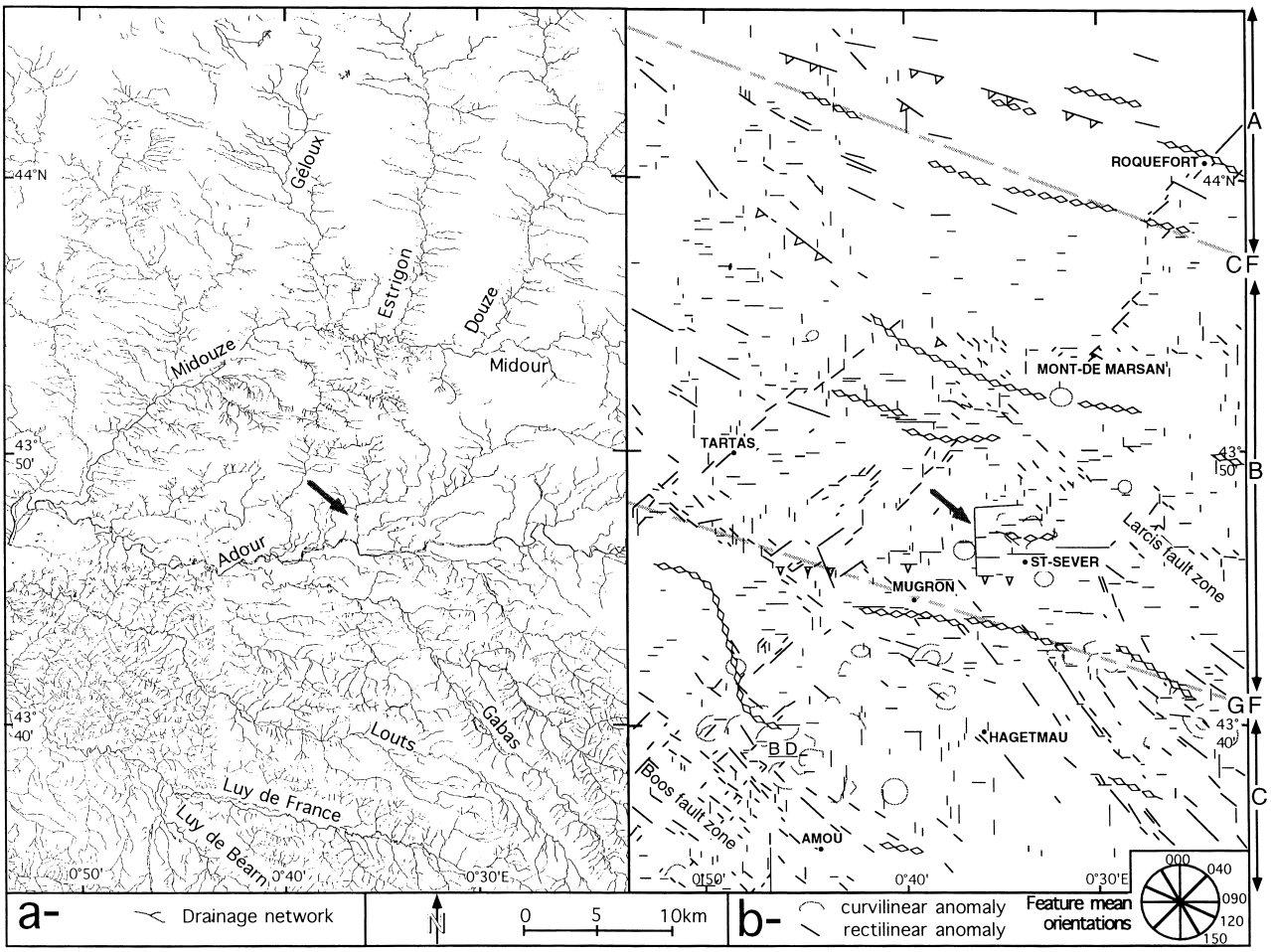

Fig. 2. (a) Drainage network extracted from IGN 1:25 000 maps and completed with temporary watercourses and backwater deduced from topography; (b) rectilinear and curvilinear anomalies of drainage network. A, B, C: regions defined in the text; GF: 'Gasconne flexure'; CF: 'Celtaquitaine flexure'; BD: Bastennes diapir. Arrow: see text. Structural features: same key as Fig. 1(a).

N040 fractures, one of them guiding the Midouze watercourse, are identified. The C region (Arzacq Basin) is separated from the southern Mauleon Basin (D) by the N100 North Pyrenean Frontal thrust, cut by N160 and N040 strike-slip faults. The C region is characterized on the west by folds with N110 axes and parallel faults, generally corresponding to thrusts, and the NNW Boos fault zone. The eastern part of this region displays NNW major faults (for example, the Larcis fault). The bending of fold axes near these faults and the offsets of fold axes suggest a dextral movement.

Sets of subvertical faults (with rectilinear trace) with consistent azimuths and dihedral angles of about 60° are interpreted as conjugate strike-slip faults; they are generally located on the anticlines, and probably formed during and after folding. The mean direction of compression (σ_1) is thus easily identified (Fig. 3b), even though field analysis is required for confirmation (see below). To the north, two fracture sets, trending N170 and N050, form a couple of conjugate strike-slip faults consistent with a N015 compression. To the south and the southeast there are four sets of supposed strike-slip faults, trending approximately N170 and N050, N030 and E–W, which resemble two systems of conjugate faults related to N015 and N060 compressions. The N015 σ_1 direction was suspected throughout the area covered by the image; we infer that it reflects the major regional NNE Pyrenean compression. The nearly N060 σ_1 direction was recognized near some NNW major faults. This compression probably results from a local deviation of the NNE compression near the NNW-trending fault zones. This interpretation, checked with paleostress reconstructions, favours local stress perturbations during a single major tectonic event, rather than distinct events.

Drainage network and SPOT imagery analyses thus provided consistent and complementary structural information. Fieldwork and seismic studies allowed us to identify and distinguish superficial and buried structures.

2.3. Seismic profiles

The N–S cross-section of the Aquitaine region (Fig. 1b), as revealed by deep seismic profiling

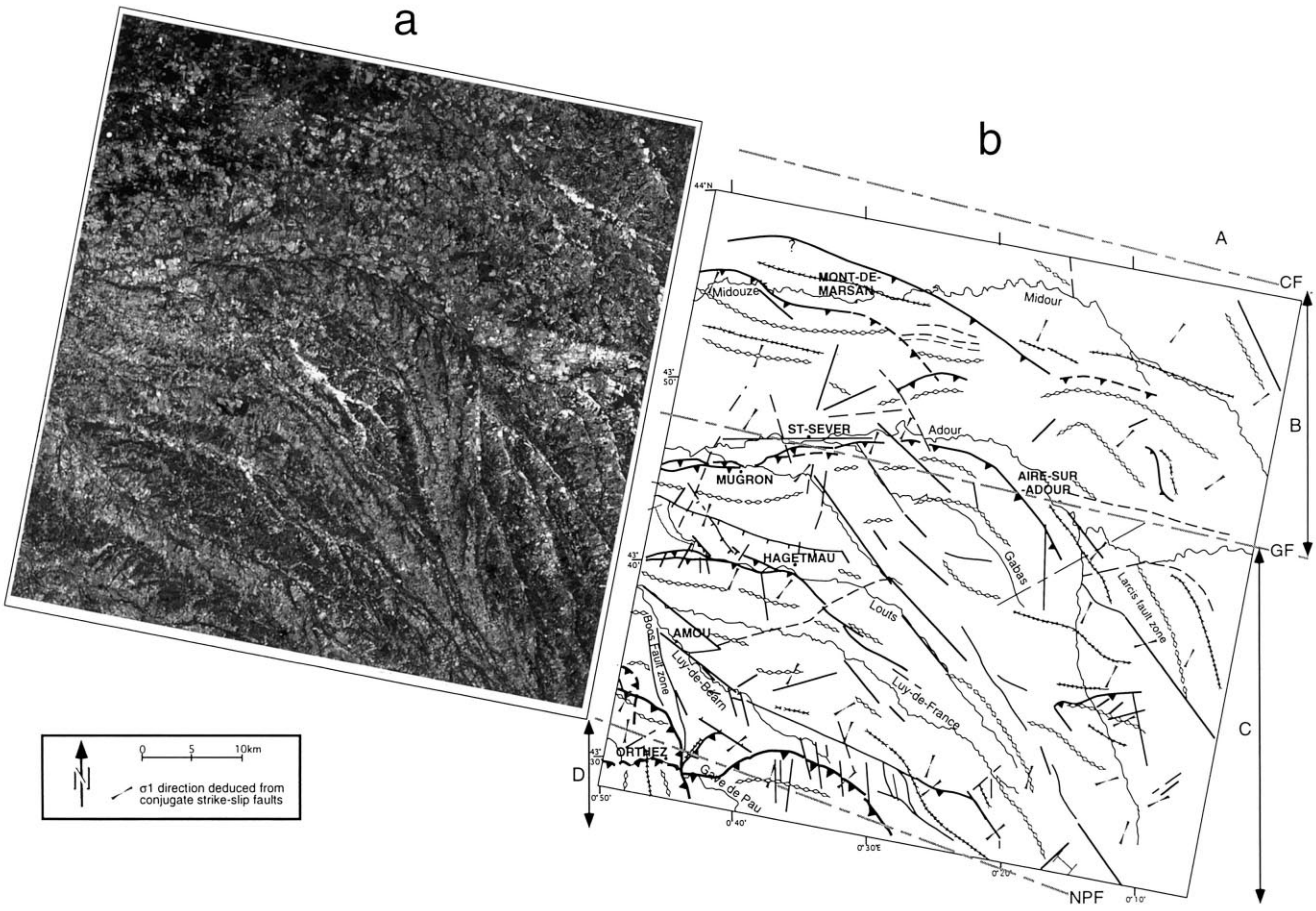

Fig. 3. (a) One SPOT image of the area (see location on Fig. 1a); (b) structures deduced from SPOT image, and σ_1 trends deduced from strike-slip faults. Structural features: see Fig. 1(a), and A, B, C, GF, CF: see Fig. 2. NPF: North Pyrenean Front; D: see text.

(ECORS Pyrenees team, 1988), show that the Pyrenees are a doubly-vergent belt. Northward from the Axial Zone, the section cuts the Mauleon Basin, the North Pyrenean fault zone and the North Pyrenean thrust zone (from St-Palais to Ste-Suzanne), then the Arzacq basin and the Landes shoal (our regions of interest). From the North Pyrenean thrust to the Landes, the fold structure is rather regular, with an average wavelength of 20 km. Most anticlines correspond to fault-propagation folds associated with north-vergent thrusts and a few backthrusts; some have localized diapirism. Thrusts may reach the surface or remain overlain by foreland Neogene deposits. They initiated upon basement faults and root in the Triassic evaporitic formations, which act as a décollement (Mathieu, 1986), or correspond to inverted N100 and N160 basement faults (Fig. 1b).

Seismic reflection profiles (Fig. 4) show that the Siougos anticline includes both a thrust and backthrusts (Fig. 4a–c). As deduced from pinching out, unconformities and variations in sediment thickness, folding was syn-depositional from the Late Cretaceous to the Oligocene (see below). Normal faulting occurs near the top of this anticline. The E–W seismic profiles (parallel to fold axis) cut numerous flower structures with reverse or normal offsets (Fig. 4d). Around these wrench zones, bulging of the Triassic formations and the overlying strata suggests a probable push-up of Triassic evaporites and clays.

This structural study was completed with structure contour maps of the K/T limit, based on seismic profiles (GDF, unpublished data); this study provides information about location of folds and occurrence of major faults, consistent with surface data.

As a result, combined fieldwork, seismic and surface data studies allowed us to construct an improved structural geology map (Fig. 5), which contains much more detail than Fig. 1(a).

3. Mechanical analysis of brittle tectonics

3.1. Inversion of fault slip data

In fault tectonics, the inverse problem consists of reconstructing paleostresses based on measurements of the directions and sense of slip along a large number of minor faults (e.g. Carey and Brunier, 1974; Etchecopar et al., 1981; Angelier, 1984, 1990). The basic principle is that the direction and sense of the observed motion along a fault plane (i.e. slickenside lineations, Fig. 6a) are parallel to the maximum shear stress exerted on it.

The computerized inversion of fault slip data yields the reduced stress tensor, including the orientation of the principal stresses σ_1, σ_2 and σ_3 ($\sigma_1 \geq \sigma_2 \geq \sigma_3$, compression positive) and the Φ ratio ($\Phi = (\sigma_2 - \sigma_3)/(\sigma_1 - \sigma_3)$, $0 \leq \Phi \leq 1$). In this study we used the INVD method of Angelier (1984, 1990). In the case of polyphase faulting, the mechanically consistent fault slips are gathered, taking into account chronological observations. Such observations deal with superimposed striations on fault surfaces (Fig. 6a), crosscutting relationships between faults, evidence for syn-depositional tectonics, time relationships between faulting and folding (Fig. 6b), etc.

The tensors are calculated for each subset of fault slips. Where tilted bedding is observed (as a result of folding), several cases deserve consideration because faults may have formed before, during or after folding. Following Anderson (1951), we assumed that one of the three principal stress axes of a tensor is generally vertical. If a fault set formed before folding and was secondarily tilted with the bedding, the tensor calculated on this set does not display a vertical axis. Instead, one of the stress axes is generally found perpendicular to bedding, whereas the two others lie within the bedding plane. Accordingly, the conjugate

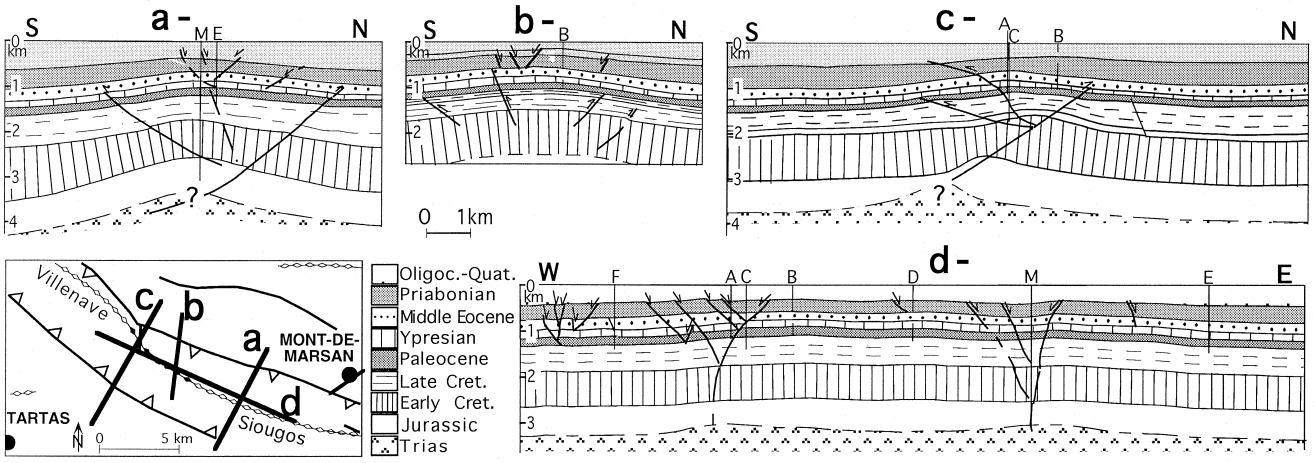

Fig. 4. Cross-sections of Siougos structure deduced from seismic reflection profiles. (a–c) N–S sections; (d) E–W section.

fault systems do not display vertical planes of symmetry. In such a case, it is necessary to backtilt the whole system (faults, tensor and bedding) in order to put it back into its initial position. Fig. 6(b) shows an example of backtilting of a fault set measured in the Tercis quarry. Note, however, that to be correct such a backtilting requires that folds be cylindrical in type with horizontal axes. Under these restrictions, this kind of analysis provides valuable information on the relative chronology between faulting events.

3.2. Inversion of calcite twin data

At low pressure and temperature, calcite aggregates deform primarily by twinning. Twin lamellae (Fig. 6c) result from the simple shear of part of host crystals along $\{01\bar{1}2\}$ crystallographic planes, called *e*-twin planes (e.g. Turner et al., 1954). Twinning occurs if the resolved shear stress τ_s acting along each *e*-plane is larger than (or at least equals) the yield stress value for twinning τ_a; if not, the *e*-plane remains untwinned. This yield stress value is nearly independent of temperature, confining and fluid pressure, but depends on grain size (Rowe and Rutter, 1990). Following Tullis (1980), Laurent (1984), and Craddock et al. (1993), we have adopted a value of 10 MPa for τ_a for a mean grain size of about 200–300 μm. For each sample, calcite twin data were collected using a Universal Stage within three mutually perpendicular thin sections.

In this paper, determination of paleostresses from twin data was performed through numerical inversion (Etchecopar, 1984), which has already led to consistent paleostress reconstructions in nonmetamorphic, weakly deformed carbonate cover rocks (e.g. Lacombe et al., 1992; Rocher et al., 1996). The tensor solution must theoretically meet the major requirement that all the twinned planes consistent with it should sustain a τ_s value larger than that exerted on all the untwinned planes. Twin data inversion provides the orientation of the principal stresses responsible for twinning (Turner,

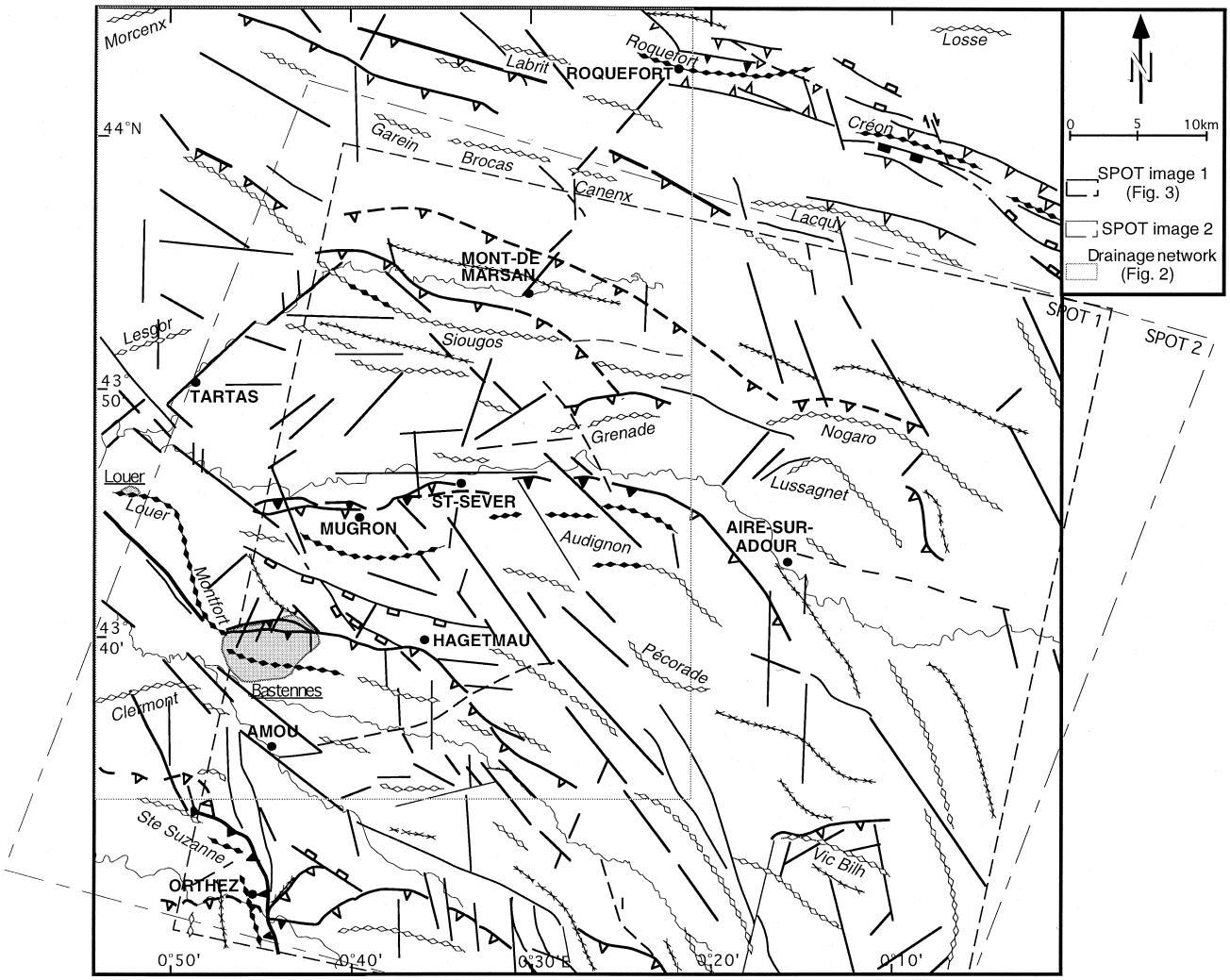

Fig. 5. Synthetic structural map of the studied region (compare to Fig. 1a). Structural features: same key as Fig. 1(a).

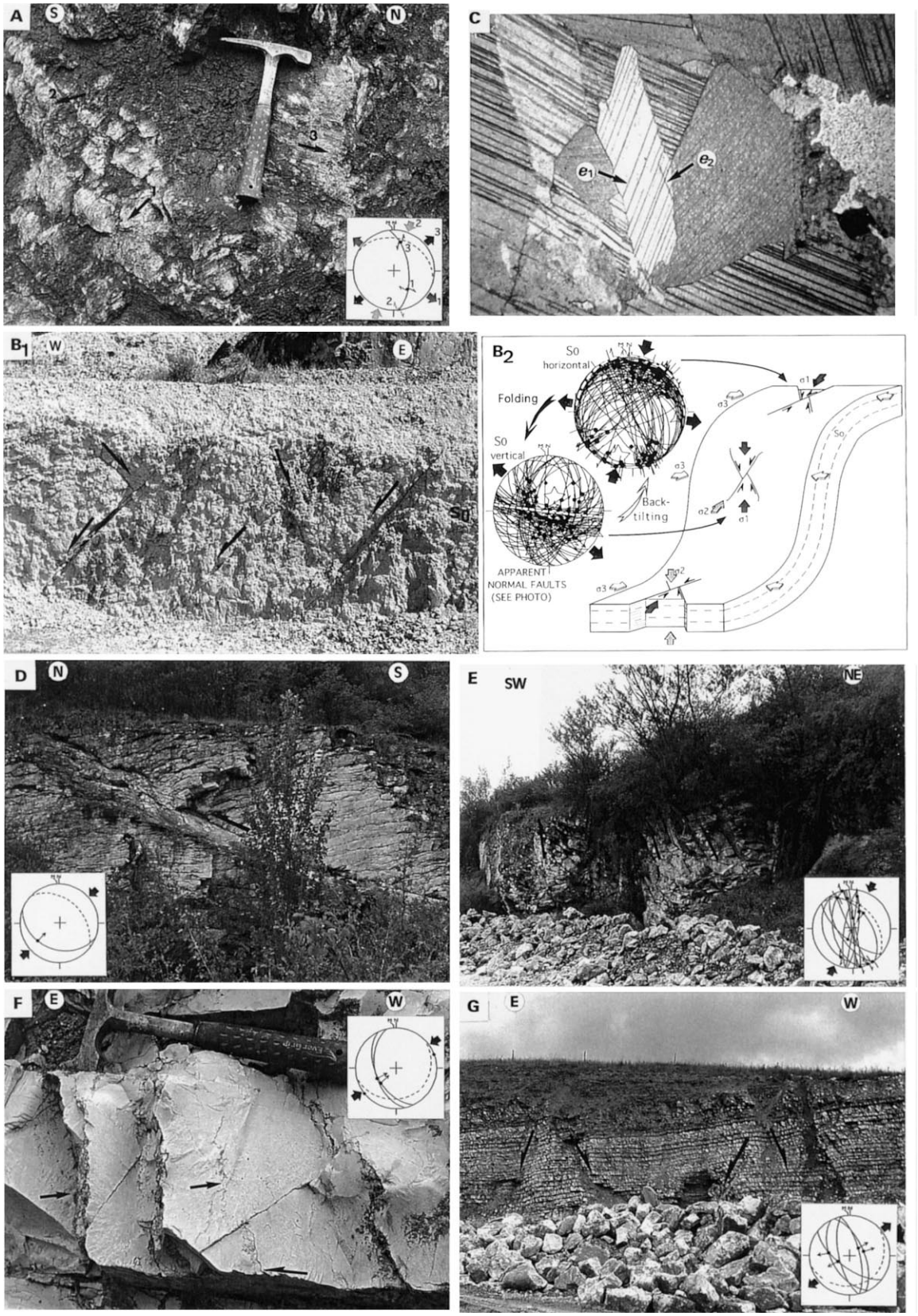

Fig. 6. Photographs. A—Cross-cutting striae on a large fault plane within Urgonian limestones on Sainte-Suzanne anticline. B—Tilted strike-slip faults in Tercis quarry, and principle of backtilting for fault set measured (S_0: bedding plane). C—Example of measured mechanical twin sets in calcite. D—Reverse fault in the La Ménière quarry; E—Flower structure in La Ménière quarry; F—Stylolites associated with bedding-parallel slips in Loubieng quarry; G—Late normal faults in Loubieng quarry. Diagrams: thin curves represent fault planes, and dots with double arrows (left- or right-lateral) or simple ones (centrifugal-normal; centripetal-reverse) indicate slickenside lineations. Stars indicate stress axes with five points (σ_1), four points (σ_2), and three points (σ_3). Empty squares represent poles to tension gashes. Full lozenges represent stylolitic peaks. Bedding planes (S_0) shown as dashed lines.

1953; Dietrich and Song, 1984; Pfiffner and Burkhard, 1987; Lacombe and Laurent, 1992; Craddock et al., 1993), the Φ ratio, and an intra-program value of the yield stress, $\tau_{a'}$, (Etchecopar, 1984; Tourneret and Laurent, 1990), which corresponds to the lowest τ_s value sustained by the twinned planes accounted for by the tensor solution, for a differential stress $(\sigma_1 - \sigma_3)$ scaled to 1 $[(\sigma_1 - \sigma_3)^* = 1]$. The fifth parameter $(\sigma_1 - \sigma_3)$ (MPa) of the tensor can thus be determined as follows:

$$(\sigma_1 - \sigma_3) = \frac{\tau_a}{\tau_{a'}} \times (\sigma_1 - \sigma_3)^* = \frac{10}{\tau_{a'}}. \quad (1)$$

If many twins are found that are not consistent with a stress tensor, the process is repeated with these inconsistent twinned planes and the whole set of untwinned planes. In case of polyphase tectonism, such a separation of superimposed stress tensors has provided consistent results with independent stress reconstructions from polyphase fault sets in the same sites (e.g. Lacombe et al., 1992).

As shown by Rocher (1999), determination of superimposed stress tensors by the Etchecopar method (1984) is particularly reliable (less than 5° of error on the principal stress axes orientations, and less than 0.1 on Φ). The $(\sigma_1 - \sigma_3)$ magnitude is generally well defined for the first tensor determined, but separation of states of stress may induce a maximum error of 50% in the magnitude of the successive tensors; these values are therefore considered herein as rough estimates of differential stress magnitudes.

In case of folding, the principle of backtilting stress tensors is the same as for fault slip analysis: the backtilted solution is retained provided that the orientation of stress axes is significantly improved with respect to the horizontal and/or vertical.

3.3. Paleostress reconstructions in the Mont-de-Marsan region

In the Mont-de-Marsan region, paleostresses were reconstructed using both fault slips and calcite twins.

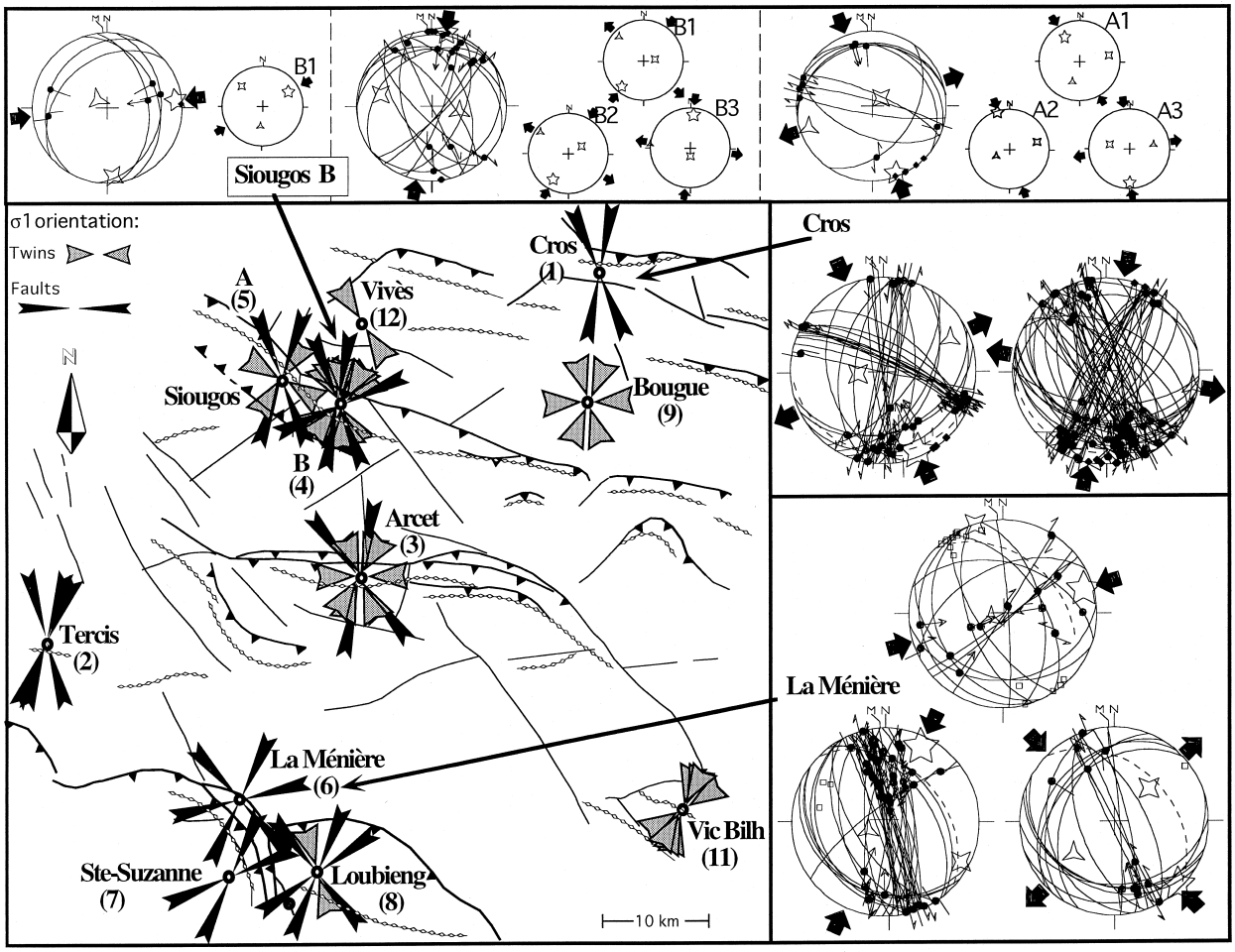

Fig. 7. Compressional states of stress deduced from calcite twins and fault slips. Large diagrams: faults, small diagrams: twins (same key as Fig. 6).

Four important sites located on N110-trending anticlines allowed observation of fracture patterns: the quarries of Cros, Tercis and Arcet, and the cores of two wells on the Siougos anticline (Figs. 7 and 8, Table 1). Ten calcite samples were collected in the Arcet, Sarraziet, Vivès and Bougue quarries, and in the cores from Siougos (Figs. 7 and 8, Table 2).

Fault measurements in the Cros quarry (Fig. 1a, Table 1) were made on Coniacian limestones, dipping 30° to the north. Conjugate wrench faults and reverse faults associated with stylolites indicate a NNE and a NNW compression (Fig. 7). Crosscutting striations on fault planes indicate that the NNW compression postdated the NNE compression. The NNW compression (with reverse faults, Fig. 7) progressively evolved into a strike-slip regime with σ_1 trending NNW and σ_3 trending ENE ($\sigma_2 - \sigma_3$ permutation) and finally into an ENE extension ($\sigma_1 - \sigma_2$ permutation, Fig. 8), as deduced from evolution of pitch of striations on a same fault plane, or along parallel fault planes (Guimerà, 1984). Minor newly formed normal faults related to this late extension cut all previous structures.

In the Tercis quarry (Fig. 1a, Table 1), Campanian to Maastrichtian vertical limestone strata trend N100. Some Triassic clays were observed on the outcropping core of the Tercis fold, relayed to the east by the Dax diapir. Most faults are strike-slip or reverse in type and associated with layer-parallel slips, consistent with a NNE compression predating folding: we presently observe N120 normal faults dipping 70° to the south, and N020 normal faults dipping 45° to the east or to the west, which respectively correspond after backtilting to N110 reverse faults, and N030 dextral and N170 sinistral strike-slip faults (Fig. 6b). Some strike-slip and reverse faults yield a NNE compression post-dating folding (these faults formed in the position in which they are presently observed). Many stylolitic joints, with dips from 0 to 90°, are consistent with the NNE compression; oblique ones having formed during strata tilting. This indicates that the NNE compression, which is perpendicular to fold axis, prevailed before, during and after strata tilting and is therefore responsible for both folding and contemporaneous faulting. Some other post-folding states of stress were reconstituted (Table 1): a NNW compression, followed by a perpendicular ENE extension, then a minor ENE compression. A NW–SE extension was also reconstituted but relative dating of this event was not possible.

The Arcet quarry (Fig. 1a, Table 1) consists of Danian dolomitised limestones with bedding striking N090 with dip of 30°N, unconformably covered by Oligocene deposits. Large vertical faults correspond to

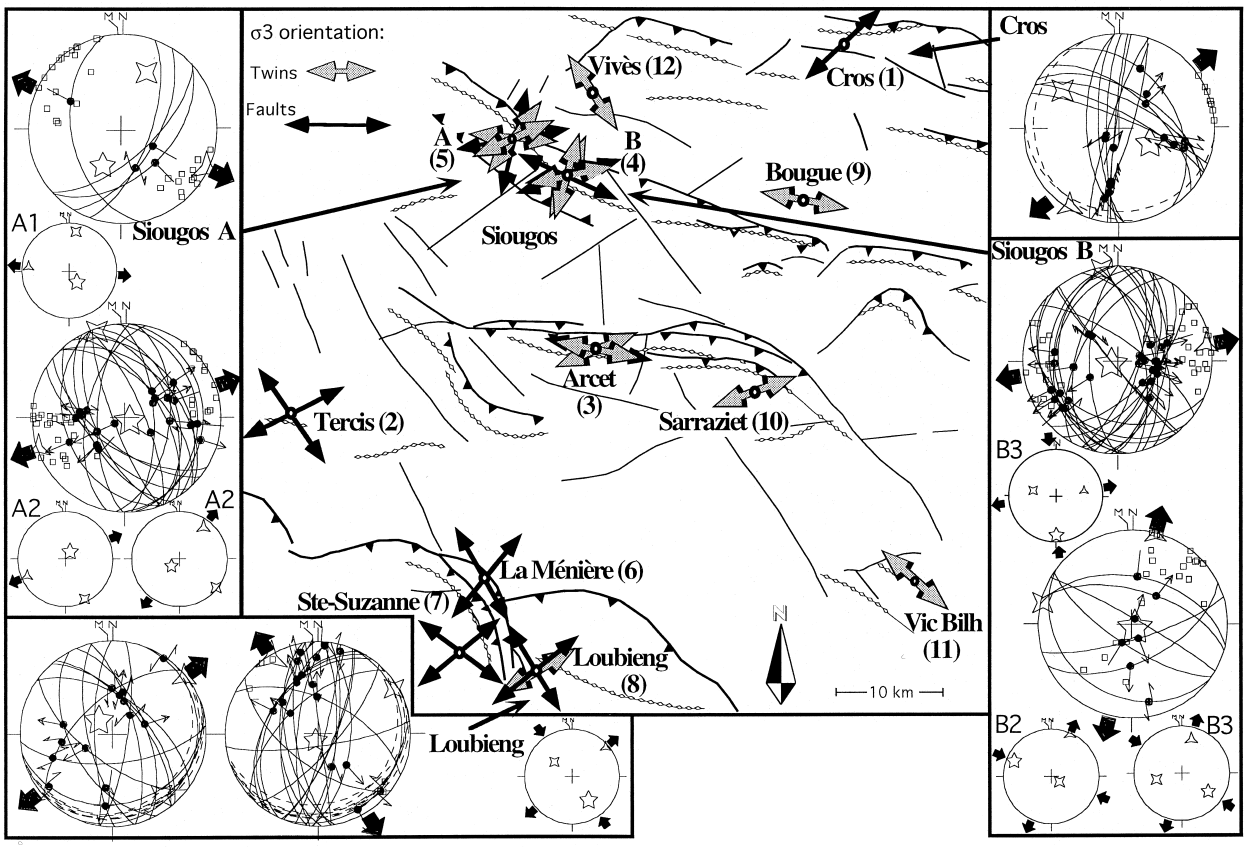

Fig. 8. Extensional states of stress deduced from calcite twins and fault slips. (Same keys as Figs. 6 and 7.)

two conjugate strike-slip fault systems, trending N–S and N120, and N160 and N040, consistent with a NNW compression and a NNE compression, respectively. These faults underwent a later opening and filling from edges to centre with calcite, aragonite and clays.

Two oriented drill-cores from the axial zone of the Siougos anticline (Fig. 1a, Table 1) were also studied. Fault slip data were collected in these Danian to Ypresian limestones. We determined (Figs. 7 and 8) a NNE compression with reverse faults, a strike-slip regime with σ_1 trending NNE and σ_3 trending WNW, and a NNW compression characterized by reverse and strike-slip faults and sub-horizontal stylolitic peaks. Two nearly E–W extensions (ENE and WNW) were also detected, with strike-slip and normal faults associated with sub-vertical stylolitic peaks. A minor ENE compression is marked by a few stylolites and a N–S extension has generated faults and tension gashes. Superimposed striations on fault planes show that the NNE compression pre-dates the NNW compression. Systematic cross-cutting of horizontal stylolitic peaks, consistent with sub-meridian compressions (NNE and NNW), by vertical stylolitic peaks (ENE extension), proves that these compressions pre-dated the ENE extension.

The ten calcite samples collected from rock matrix or veins over the whole region showed optimal conditions for twin analysis: calcite grains of nearly homogeneous size (200–500 μm), with rare impurities and randomly distributed optical axes. Some samples were extracted in quarries where faults were also measured (Arcet and Siougos anticlines), which provided an independent mutual control on paleostress determinations. Samples extracted at Bougue, Sarraziet and Vivès (Fig. 1a) provided paleostress information, even where no fault was observed.

Two calcite samples were extracted from large sub-

Table 1
Stress tensors (in the order of description in the text) determined by inverse analysis of fault slips. *C*: chronological order (see text); σ_1, σ_2, σ_3: principal axes of the stress tensor (trend-plunge in degrees); Φ: ratio $(\sigma_2-\sigma_3)/(\sigma_1-\sigma_3)$; α: mean angle between observed stria-computed shear; *N*: number of data; RUP: estimator of Angelier's program (1990); Q: quality of the result (A: good, B: intermediate, C: poor)

Site	*C*	σ_1	σ_2	σ_3	Φ	α	*N*	RUP	Q
Cros	1	191-09	335-79	100-06	0.2	13.4	59	43	A
(1)	3	157-06	262-68	065-21	0.2	11.0	37	33	A
CONIACIAN	?	115-38	254-44	007-22	0.2	17.7	7	46	C
	2?	116-61	304-29	212-19	0.5	19.1	15	49	B
Tercis	1	025-69	205-21	115-00	0	11	76	31	A
(2)	*1*	*196-19*	*334-66*	*100-15*	*backtilted tensor*				
MAASTRICH.–CAMPANIAN	2	025-10	292-12	153-74	0.4	13	11	43	B
	3	164-19	356-70	255-04	0.2	17.1	17	39	B
	4	203-74	331-10	063-12	0.6	13.5	10	39	B
	?	288-78	055-07	146-09	0.9	14.1	17	37	B
Arcet (3)	1	191-04	018-85	281-01	0.5	7.3	4	28	C
DANIAN	2	142-19	324-71	232-01	0.8	9.1	6	27	B
Siougos Well B	1	012-02	281-30	105-60	0.2	18	13	45	B
(4)	3	159-05	046-78	250-11	0.2	21.5	12	42	B
PALEOCENE	4	234-84	350-03	080-05	0.4	15.6	26	32	A
	2	146-87	284-03	014-02	0.2	19	7	46	B
	?	246-03	337-23	149-67	0.3	8.8	5	40	B
Siougos Well A	1	199-05	305-71	107-18	0.6	18.0	7	41	A
(5)	3	160-07	335-83	070-01	0.5	14.5	12	45	B
PALEOCENE	2	208-54	023-36	115-03	0.7	6.4	4	28	C
	4	135-85	341-04	251-02	0.4	11.3	20	29	A
La Ménière	1	076-13	346-02	246-77	0.2	19.4	13	47	C
(6)	2	195-77	062-09	330-09	0.7	7.8	13	35	A
MAASTRICH.–CAMPANIAN	3	024-14	116-10	241-73	0.2	21.3	40	40	A
	4	135-05	039-48	229-41	0.1	17.1	11	47	C
	5	152-78	308-11	039-05	0.5	18.5	15	45	C
Sainte-Suzanne	1	247-04	339-20	148-69	0.5	16.6	14	35	B
(7)	2	244-66	033-20	127-11	0.5	14.7	16	43	B
URGONIAN	3	204-12	297-14	075-72	0.1	10.4	9	34	B
	4	153-77	318-12	049-03	1	11.6	5	30	C
Loubieng	1	235-04	143-27	332-63	0.5	15.6	15	43	B
(8)	2	200-84	059-05	329-04	0.8	1.2	16	46	C
DANIAN	3	022-01	291-52	113-38	0.2	15.1	66	36	A
	4	141-09	049-11	269-75	0	21.7	40	51	B
	5	313-73	142-17	051-02	0.4	16.2	14	45	B

Table 2
Stress tensors (in the order of description in the text) determined by inverse analysis of calcite twins. Age: age of sampled formation; σ_1, σ_2, σ_3, Φ and Q: see Table 1; MT, NT: respectively total number of twinned and untwinned planes; M; N: respectively number of twinned and untwinned planes consistent with the result; $\tau_{a'}$: intra-program value of the yield stress (see text); σ_{1D}: deviatoric component of σ_1

Site and Age		σ_1	σ_2	σ_3	Φ	MT	NT	M	N	$\tau_{a'}$	σ_{1D}	Q
Bougue		204-13	089-61	300-25	0.5	121	26	58	24	0.08	107	A
(9)		088-09	221-77	356-09	0.3	65	24	27	23	0.16	48	A
OLIGOCENE		343-22	246-17	122-61	0.1	41	21	19	21	0.27	27	C
Arcet	1	031-50	301-01	210-40	0.7	100	24	35	24	0.14	62	A
(3)		*021-23*	*118-14*	*236-68*	*backtilted tensor*							
DANIAN		153-01	243-21	061-69	0.3	67	22	24	21	0.20	38	B
		091-03	182-21	352-69	0.5	43	22	20	21	0.10	80	C
		190-21	015-69	281-01	0.9	24	21	17	20	0.24	40	C
	2	033-30	236-58	129-10	0.3	81	33	41	33	0.11	71	A
		159-06	264-68	067-21	0.4	43	30	17	30	0.24	32	C
Sarraziet (10) PALEOCENE		000-51	149-35	250-16	0.5	129	42	49	36	0.14	52	B
Siougos Well B	1	057-31	312-24	191-49	0.2	157	29	39	29	0.25	30	A
(4)		211-26	060-61	307-12	0.3	120	27	39	27	0.21	37	A
PALEOCENE		329-32	076-25	197-47	0.2	84	24	33	22	0.23	32	C
	2	342-06	075-30	241-59	0.3	132	45	46	41	0.17	47	B
		219-17	082-68	313-14	0.4	86	45	38	39	0.20	40	B
		125-33	256-45	016-27	0.5	50	43	25	36	0.21	40	C
	3	293-17	123-73	024-03	0.4	89	17	35	17	0.13	61	A
		006-18	178-72	276-02	0.1	55	16	26	16	0.22	33	A
		178-11	281-48	079-40	0.5	30	15	14	15	0.07	101	C
Siougos Well A	1	146-66	010-18	275-15	0.3	125	38	56	38	0.14	54	A
(5)		123-20	255-62	026-19	0.2	69	38	24	35	0.22	34	B
PALEOCENE	2	033-75	154-08	246-13	0.3	120	36	54	35	0.12	63	A
		213-27	059-60	309-11	0.2	68	34	37	33	0.18	40	B
		229-72	128-03	037-18	0.6	32	33	15	33	0.23	39	C
Loubieng		145-39	310-50	049-7	0.2	125	47	45	42	0.26	29	A
(8) DANIAN		337-13	242-22	095-65	0.6	84	43	29	42	0.23	38	C
Vic-Bilh	1	060-34	168-24	285-46	0.1	50	55	15	53	0.30	24	B
(11)		210-57	082-22	342-23	0.4	35	55	14	51	0.26	31	C
KIMMER.	2	016-23	275-24	143-56	0.1	46	89	36	85	0.17	42	A
	3	205-03	076-47	312-27	0.4	107	49	64	46	0.12	68	A
	4	032-02	122-01	012-88	0.4	74	58	51	58	0.09	80	A
Vivès (12)		164-61	059-09	324-28	0.4	96	32	41	31	0.12	34	A
MIOCENE		328-16	058-03	158-74	0.9	58	29	25	28	0.34	26	C

vertical fractures trending N020 of the Arcet quarry. The NNE compression determined in both samples (Table 2) probably generated these N020 cracks. In the sample Arcet 1 a pre-tilting and a post-tilting NNE compression was determined, which is thus inferred to be responsible for tilting of bedding. In both these samples we also determined a NNW compression.

The calcite sample of Sarraziet quarry (Fig. 1a, Table 2) was collected from a vertical N150-trending tension gash, in the same material as in Arcet. A N070 extension was established (Fig. 8), which was probably responsible for the fracture opening.

In the Bougue sample, twin data were collected from the rock matrix of Oligocene limestones. The sample has recorded three states of stress (Table 2, Fig. 7), a striking result in such recent formations, where no fault is observed. The most important corresponds to a stress regime with σ_1 NNE and σ_3 WNW, consistent with a previously identified regional strike-slip regime. It is supported by N030–050 normal faults in the Oligocene sandy molasses of the Arcet quarry and N040–050 joints in Aquitanian formations at Roquefort, consistent with an Oligo-Miocene WNW extensional strike-slip regime.

At Siougos, we extracted two samples in the first well (A) and three in the second (B) (Fig. 1a, Table 2). The sample B1 and B3 showed sparry calcite in the rock matrix. Samples A2 and B2 were collected from cracks filled with calcite, respectively oriented N108, 73°S and N128, vertical. The sample A1 is a calcite-filled hole. Results are consistent with fault slip data inversion (Figs. 7 and 8).

Summarizing, a major NNE compression was widely identified (Fig. 7). At the outcrop scale, it corresponds to N110 reverse faults and folds, and to NE–SW (sinistral) and NNW (dextral) strike-slip faults. This can be extrapolated to the regional scale by considering that NNW and NE–SW faults, mapped from analyses of surface data, are also strike-slip faults. N150–170 strike-slip faults are responsible for local bending of anticline axes. All the other recognized paleostress states occurred after folding. The NNE compression was followed by a NNW compression (Fig. 7). Under a late ENE extension, many strike-slip faults generated by the earlier compressions were reactivated as normal faults, and new N160 normal faults developed. In addition to these major tectonic regimes, a local NNE extension occurred at the hinge of Siougos anticline, simply because of lengthening on the convex side of folded series. The minor post-folding WNW extension (Fig. 8), pre-dating the NNW compression and the ENE extension, may correspond to stress relaxation after the NNE compression.

The complex relationships between folding, NNW fracturing and stress field required study of other structures. The Audignon anticline certainly formed in relation to NNW wrench faults (Fig. 1a) but no quarry or well has an appropriate location for observation. We have consequently focused on a genetically similar structure, outcropping along the North Pyrenean Front, the Sainte-Suzanne anticline (Fig. 1). Extending the paleostress analyses to this southern region will also allow confirmation of the regional significance and the chronology of the two successive directions of compression (NNE and NNW) determined near Siougos, and the meaning of the WNW and ENE extensions.

3.4. Paleostress reconstructions along the North Pyrenean Front

The Sainte-Suzanne anticline formed along the North Pyrenean frontal thrust. The fold axis is oriented N110 and turns to the southeast to N170, near Orthez (Fig. 1a). Syn-folding deviation of the anticline axis seems to be related to a large N170 fault zone, probably inherited from the Hercynian orogeny and Mesozoic extensions and injected with Triassic salt. Three sites were studied along the eastern part of the anticline, where the fold axis trends N170: Loubieng and La Ménière quarries, and Sainte-Suzanne outcrop. The results of fault slip analyses are compared to the results of calcite twin data inversion from one sample taken at Loubieng, and to the work carried out by Tourneret (1990) from Vic Bilh cores.

In La Ménière quarry (Fig. 1a), Maastrichtian limestones beds trend N140 and dip NE from 30° to 50° as one progresses from west to east. Shallowly dipping thrust planes (Fig. 6d) are observed on the west and east walls. A large fracture zone, marked by bedding parallel slips and subvertical N170 fracture cleavages with strike-slip reverse striations indicate transpressional deformation (Fig. 6e). Some late normal faults cut all previous structures, but others developed rather early. Inversion of fault slip data and separation of data subsets based on relative chronology criteria suggest the following succession: an ENE compression responsible for folding, then a perpendicular NNW extension, a NNE compression with reverse faults and numerous dextral N170 faults, then a NNW minor compression followed by a perpendicular ENE extension (Fig. 7).

In Loubieng quarry (Fig. 1a), N050-trending Danian limestones dip 15°S. Sigmoidal intraformational stylolite duplexes (Fig. 6F) and slumps are consistent with an early ENE compression. A minor NNW extension generated normal faults cutting the previous sigmoid planes (Fig. 8). Later a NNE compression prevailed, marked first by reverse faults, followed by strike-slip faults (numerous dextral faults trending N170). Subsequently, a new NNW-directed compression affected limestones with reverse and strike-slip faults. Some late

normal faults are consistent with an ENE extension (Figs. 6g and 8).

The Sainte-Suzanne anticline locally crops out (Fig. 1a) as Urgonian limestones, trending N150 and dipping 25° NE. A large N170 subvertical fault plane strikes parallel to the nearly N170 basement faults reactivated as strike-slip faults and responsible for the bending of the fold axis. This plane displays several generations of striae (Fig. 6a): some striae indicating a reverse sense of slip (ENE compression) are cut by normal striae consistent with a NW–SE extension, which are cut by striae indicating dextral slip associated with a NNE compression; some normal striae consistent with an ENE extension post-date all previous ones. No NNW compression has been identified.

Only one calcite sample was collected from a calcite-filled tension gash in the Loubieng quarry. Two tensors were determined: a NNW strike-slip compression, and a ENE extension (Fig. 8). Tourneret (1990) also carried out inversion of calcite twin data from cores from Vic-Bilh field (Elf-Aquitaine); the tensors determined also indicate ENE, NNW and NNE compressions (Table 2).

As a result, the NNE and NNW compressions and the ENE extension determined in the region of Mont-de-Marsan have also been recognized along the North Pyrenean front. They thus correspond to regionally significant states of stress. Chronology between these events has been confirmed: NNE then NNW compression, followed by ENE extension (e.g. Fig. 6a). However, additional early events were reconstituted locally around Orthez: an ENE compression and a NNW extension. The ENE compression should correspond to the NNE major compression reoriented perpendicularly to fold axis, locally trending N170. This state of stress had been previously suspected by analyses of strike-slip faults on SPOT images in regions where NNW major faults exist (Fig. 3b). This could explain similar local observations in the Cros and Siougos sites. The NNW extension may be interpreted as being due to local stretching along N170 fold axis, which in turn is due to northward migration of the Pyrenean front.

4. Dating of tectonic events

Dating of identified tectonic events deserves detailed consideration. Various types of data may provide time constraints on deformation, such as consideration of the age of the folded-faulted formations or characteristics of sedimentary formations (syntectonic deposits, hiatus, bevelments); additional information comes from evolution of folding through time, deduced from calculation of shortening rates on seismic profiles, or from variations in strata thickness with distance to the top of anticlines on wells.

Regarding the age of the folded-faulted formations, the NNE compression has been detected in Late Cretaceous to Oligocene formations (Tables 1 and 2), but not in the Miocene (Roquefort and Vives quarries). We conclude that it persisted until the Oligocene.

Cenozoic stratigraphy studies in the South-Aquitaine Basin (Sztråkos et al., 1997, 1998) reveal major erosional events related to Pyrenean shortening. Minor early events occurred during the Maastrichtian (65 My), the Middle Thanetian (58 My) and the Late Thanetian (56 My); major episodes correspond to the 'I, II and III Palassou phases' (Ypresian, 53 My; Ypre-

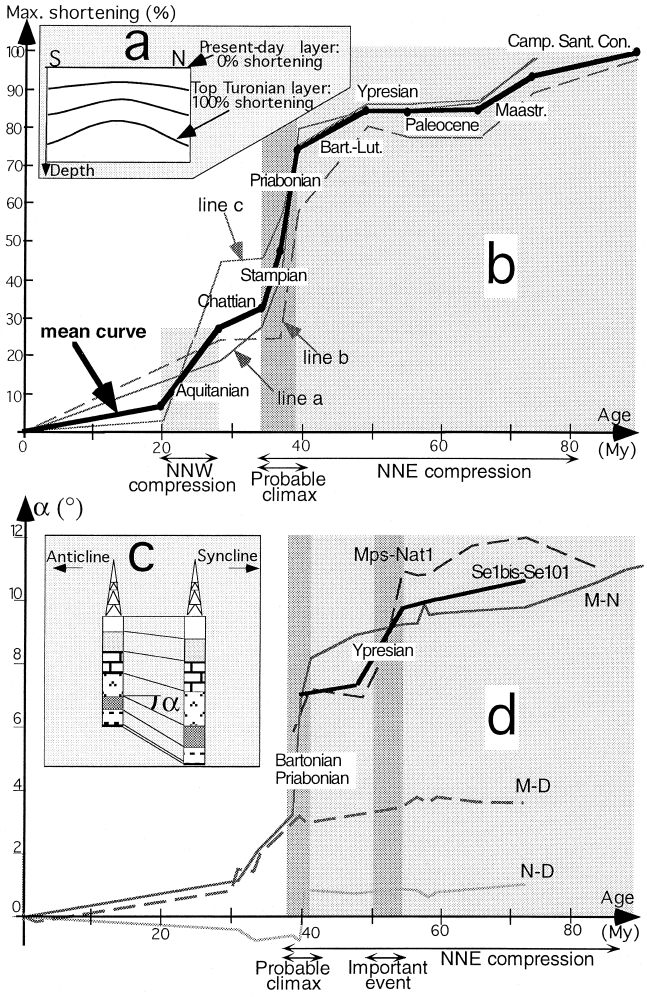

Fig. 9. (a) Example of shortening analysis on a depth-migrated seismic profile; (b) mean curve of N–S shortening with time of the Siougos structure, from analysis of three N–S-trending profiles (Fig. 4a, b, c); (c) example of analysis of strata thickness variation vs. distance to an anticline. α: dip of the line between the tops of each strata; (d) variation of α with time, for three couples of wells on the Siougos structure (M–N, N–D, M–D), one couple on the Sebastopol structure (Se1–Se101), and one couple on the Bastennes structure (Mps–Nat1). Note the rapid increase in shortening during the Late Eocene.

sian–Lutetian, 48.5 My; Late Bartonian–Priabonian, 38. 5 My) (Cavelier et al., 1997). A late tectonic event may occur during the Early Rupelian (33 My). Such studies are consistent with age estimates of thrusting events by Déramond et al. (1993) in the Central Northern (and Southern) Pyrenees.

Time distribution of deformation of the Siougos anticline was examined using three seismic profiles perpendicular to the fold axis (Fig. 4a, b, c). On each depth-migrated profile, the lengths of 11 chosen layers were measured, ranging in age from the Coniacian to Present. The oldest layers are the longest and most curved (folded), whereas the recent ones are less and less curved and long (Fig. 9a). When the Coniacian base layer is backfolded to horizontal, we observe that older layers are also horizontal. We thus assume that the base of the Coniacian corresponds today to 100% of maximum shortening. We can therefore elaborate a mean curve of shortening evolution with time (Fig. 9b). The total shortening is about one kilometre. Because of uncertainties on measurements, a maximum error of 10% shortening can be attributed to each length. In Fig. 9(b), we observe that shortening began at Middle Senonian, then stopped until Lutetian, and became more and more important, till the Priabonian, when it is paroxysmal. The contraction then decayed, with a new start during the Aquitanian. The NNE compression achieved during the Oligocene (see this section, ages of the outcrops), and the slight increase in shortening during Aquitanian may thus be related to the NNW compression.

Another way to determine the evolution of syndepositional folding through time is to study the variation of sediment thickness with distance to the anticlines in that during syndepositional folding, the sedimentation rate is greater in synclines than in anticlines (Fig. 9c). By comparing the thickness of each stratum between two wells situated at different distances from an anticline, a curve of the evolution of this fold through time can be drawn (Fig. 9c). Five curves were constructed (Fig. 9d), with three pairs of wells on the Siougos structure, one pair on the Sebastopol structure, and one pair on the Bastennes structure (Fig. 1a). Curves obtained this way for the Siougos structure are consistent with those obtained from seismic studies (Fig. 9b), with a major compression during the Late Eocene. For the Sebastopol and Bastennes structures, the same major Late Eocene compressive event and an additional Ypresian event were detected. The record of this earlier compressive event in the Sebastopol and the Bastennes sites, situated nearer to the Pyrenees than Siougos, supports the progressive migration, albeit discontinuous, of deformation from the belt toward the foreland.

The Ypresian and Late Eocene compressive events respectively correspond to the 'Palassou II' and 'Palassou III' tectonic events identified by analyses of syntectonic formations.

5. Quantifying paleostress magnitudes from calcite twin data

The intensity of the Pyrenean deformation decreases northwards, with a rapid attenuation across the foothills from the Axial Zone of the Pyrenees to the North Pyrenean front, and a more distributed decay in the Pyrenean Foreland from the Landes Shoal to Paris Basin (Lacombe et al., 1996). Calcite twin analysis was used to estimate the northward evolution of stress in the Aquitaine Basin.

As previously mentioned, a constant value of 10 MPa is adopted for the yield stress of twinning τ_a (Eq. 1), for a mean grain size of 300 μm. The deviatoric component of stress σ_1 (Table 1) is therefore determined as follows:

$$\sigma_{1D} = \sigma_1 - (\sigma_1 + \sigma_2 + \sigma_3)/3 = [(\sigma_1 - \sigma_3)(2 - \Phi)]/3$$
$$= 10(2 - \Phi)/(3\tau_{a'}). \quad (2)$$

Remembering the significance of $\tau_{a'}$, if the number of untwinned planes identified in a polyphase sample is very low, the twinned planes included in the solution are too numerous, so that the $\tau_{a'}$ value is underestimated; the differential stresses are consequently overestimated (Eq. 1). Some overestimated values of σ_{1D}, greater than 100 MPa, were obtained for this reason (Eq. 2) from the samples of Bougue and Siougos A3, in which untwinned planes represent 18% or less of the measured twin planes (Table 2).

For the NNW compressional tensor, the value of σ_{1D} is 35 MPa on average (Table 2). The values of σ_{1D} for the NNE major compression are more variable. We observe a rapid decrease in the magnitude of NNE compressional stresses from the Pyrenean orogenic front to the foreland, suggesting an exponential decrease of σ_{1D} with the distance to the orogenic front (Fig. 10, similar to the decrease of $\sigma_1 - \sigma_3$) evidenced in the Appalachian foreland (Craddock et al., 1993). This study confirms a record of the Pyrenean stresses in the foreland at more than 700 km from the orogenic front.

The nearly NNE homogeneous orientation of σ_1 in the north Pyrenean foreland is probably related to the linear shape of the Iberia–Eurasia collisional boundary, which is nearly perpendicular to the current relative motion between plates, in contrast to the Alpine foreland where a fan-shaped distribution of σ_1 axes has been reconstructed at the front of the Apulian indenter (Bergerat, 1987). In addition, we tentatively propose that the reconstructed decreasing magnitude

of the Pyrenean deviatoric stress results from the superimposition of large local collisional stresses (70 MPa) with a rapid northwards decrease, onto nearly constant (30 MPa) intraplate stresses that reflect the plate-driving forces. The intraplate stress value thus estimated (some tens of MPa) is generally consistent with those obtained with numerical intraplate stress models (e.g. Solomon et al., 1980).

6. Interpretation of apparent numerous tectonic events and relation to plate kinematics

Numerous tectonic events can be established from our observations. A major NNE compression responsible for folding exists regionally. During this compression, a local NNE extension (Fig. 11a) may have occurred at anticline hinges. Near Orthez, the regional NNE compression deviated locally into an ENE compression (Fig. 11a) in the vicinity of a NNW pre-existing fault zone, which acted as a thrust. An early NW–SE extension, observed at Orthez, is attributed to a local stress perturbation of the ENE compression. It can be explained by a local stretching along the eastern N170 fold axis, due to the migration of the western part of the fold to the North. Later, the NNW faults underwent a dextral movement, consistent with the regional NNE compression (Fig. 11b), which evolved progressively into a strike-slip regime. During the Oligocene, a minor WNW extension (Fig. 11b) seems to be closely related to a relaxation of the NNE compression ($\sigma_1 - \sigma_2$ stress permutation). A post-Oligocene NNW compression has been detected regionally (Fig. 11c), but did not generate any major structure. The late regional ENE extension (Fig. 11c) is similarly interpreted as a $\sigma_1 - \sigma_2$ stress permutation due to relaxation of the NNW compression, and not as an independent extensional tectonic event. At the present-day, borehole breakouts (Bell et al., 1992) and focal mechanisms of earthquakes (Grellet et al., 1993) in the studied area indicate that the regional NNW compression is highly perturbed along major NE–SW and NNW faults and WNW evaporite ridges, and locally changes to a perpendicular ENE extension.

The NNE compression determined in the South Aquitaine Basin is widely recognized in adjacent regions (Arthaud and Laurent, 1995) as well as in Western Europe (e.g. Bergerat, 1987). Similar stress reorientations of the regional NNE compression into an ENE compression were observed in the Iberian Range (Guimerà and Alvaro, 1990). The succession (NNE then NNW compression) has also been recognized in Western Pyrenees (Hervouët et al., 1997), in French Béarn (Martin, 1992), in Spain (Thomas and Delfaud, 1990) and Portugal (Lepvrier and Mougenot, 1984). The NNW compression is synchronous with the deformation in the Western Alps, but the collision has continued smoothly along the Iberia–France contact until the present. Some Miocene to Pliocene nearly E–W extensions post-dating the compressions have also been determined throughout Spain (Lepvrier and Mougenot, 1984).

The major tectonic events identified through this study are thus representative of a more widespread region, and can now be placed in the framework of plate tectonics. According to several authors (e.g. Klitgord and Schouten, 1986), the pole of rotation of Africa with respect to Eurasia during the Eocene was situated northwest of Portugal, producing a N–S relative motion between Africa and Eurasia, with a boundary roughly coinciding with the Pyreneo-Alpine belt. For Oligocene times, Klitgord and Schouten (1986)

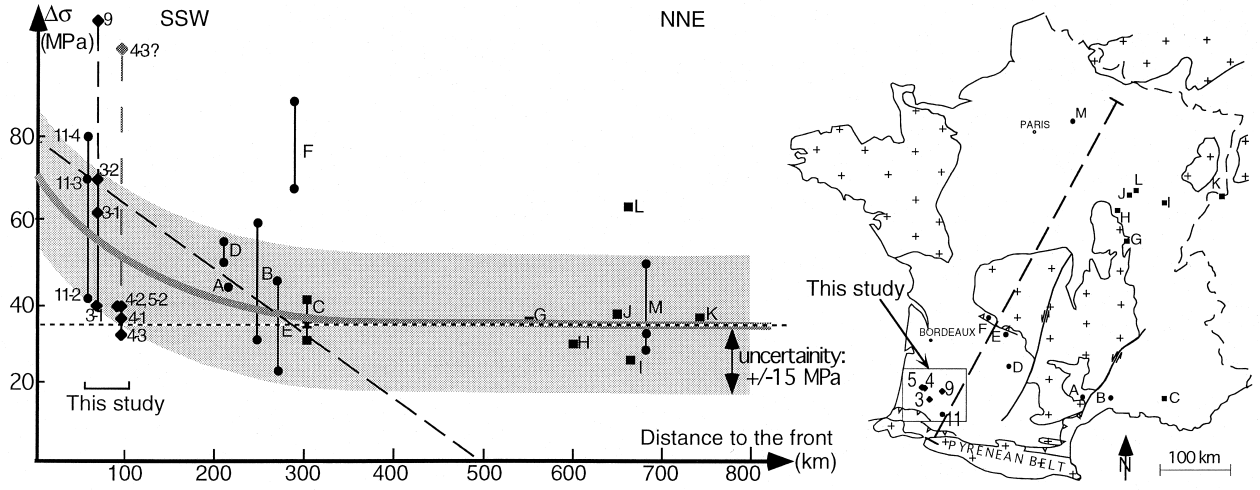

Fig. 10. Decreasing magnitude of maximal deviatoric stress σ_{1D} related to the NNE compression with the distance to the orogenic front (see map). Dashed line: collisional stresses, dotted line: intraplate stress. A to M: see Lacombe et al. (1996). 3, 4, 5, 9, 11: this study (Fig. 1a).

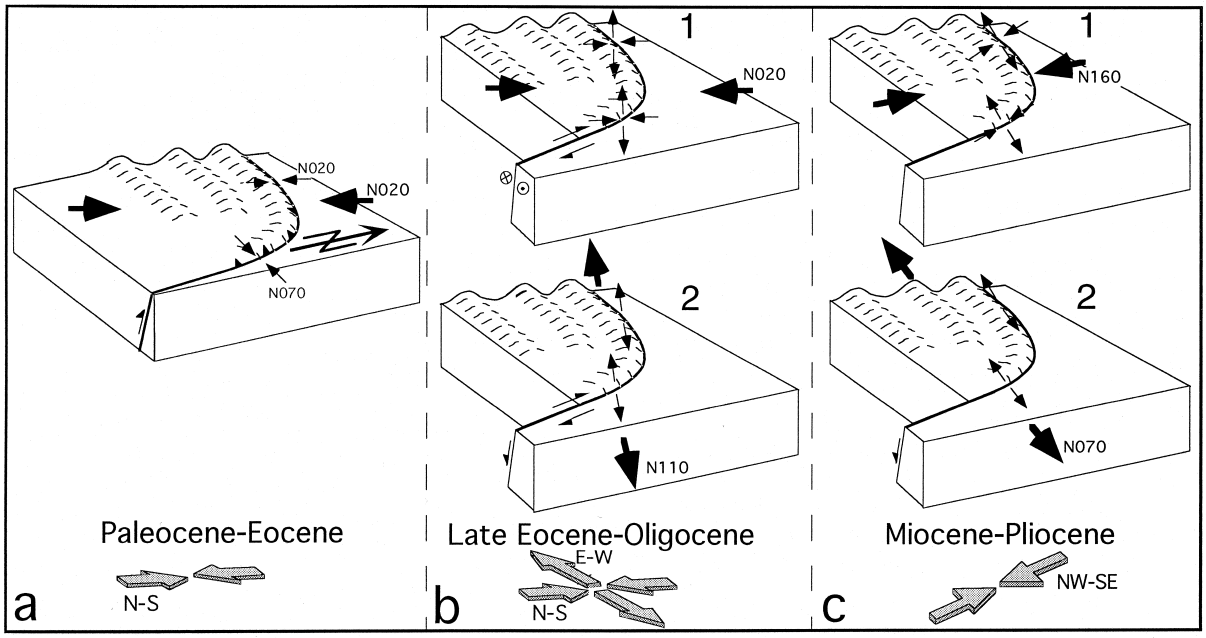

Fig. 11. Structural and paleostress evolution in the South-Aquitaine Basin, illustrated by a Sainte-Suzanne-like anticline closely associated with a N170 fold-and-thrust lateral ramp (convergent or divergent large black arrows: respectively, regional compressional or extensional states of stress; thin black arrows: local states of stress), in the framework of plate tectonics (large grey arrows: relative plate motion).

determine a relative southward motion of western Eurasia with respect to Africa. A lateral stress relaxation can be deduced from the difference of motion between western Eurasia and the remainder of the Eurasian plate (Le Pichon et al., 1988). For Miocene times, the motion of western Eurasia with respect to Africa is southeastward (Klitgord and Schouten, 1986).

The results of our tectonic analyses are thus consistent with all regimes predicted by plate tectonics models. Considering the rectilinear plate boundary, nearly perpendicular to the convergence vector between plates during the Eocene, the relative N–S plate convergence is generally consistent with the Pyrenean NNE compression (Fig. 11a). For the Oligocene, a NNE compressive strike-slip regime and a WNW extension are also consistent with the motion of western Eurasia with respect to Africa (Fig. 11b). For Miocene times, the NNW compression determined in the North Pyrenean Foreland supports the southeastward motion of western Eurasia with respect to Africa (Fig. 11c).

A noticeable result of our study is that several states of stress can be related to only few tectonic events. The states of stress determined in the North Pyrenean Foreland are consistent with two major events resulting from the Eurasia–Africa plate convergence—the NNE major Pyrenean compression and the NNW Miocene compression. Rather than indicating polyphase tectonism, the complexity of the regional stress history reflects perturbations that result from local kinematics or inherited and salt-injected structures.

Acknowledgements

Fieldwork and data analyses were supported Gaz de France. The authors thank E. Leroy, K. Sztràkos and J.S. Odin for numerous discussions. Comments by J. Vergés and R.H. Groshong resulted in significant improvement of the paper.

References

Anderson, E.M., 1951. The Dynamics of Faulting, 2nd edn. Oliver & Boyd, Edinburgh.

Angelier, J., 1984. Tectonic analysis of fault slip data sets. Journal of Geophysical Research 89 (B7), 5835–5848.

Angelier, J., 1990. Inversion of field data in fault tectonics to obtain the regional stress. III: A new rapid direct inversion method by analytical means. Geophysical Journal International 103, 363–376.

Arthaud, F., Laurent, P., 1995. Contrainte, déformation et déplacement dans l'avant-pays Nord-pyrénéen du Languedoc méditerranéen. Geodinamica Acta 8, 142–157.

Autran, A., Cogné, E.J., 1980. La zone interne de l'orogène varisque dans l'Ouest de la France et sa place dans le développement de la chaîne hercynienne. In: Cogné, J., Slansky, M. (Eds.), Géologie de l'Europe, Mémoires du BRGM 108, pp. 90–111.

Bell, J.S., Caillet, G., Le Marrec, A., 1992. The present-day stress regime of the southwestern part of the Aquitaine Basin, France, as indicated by oil well data. Journal of Structural Geology 14, 1019–1032.

Bergerat, F., 1987. Stress fields in the European platform at the time of Africa–Eurasia collision. Tectonics 6, 99–132.

Boillot, G. 1984. Le Golfe de Gascogne et les Pyrénées. In: Boillot, G., Montadert, L., Lemoine, M., Biju-Duval, B. (Eds.), Les

marges continentales actuelles et fossiles autour de la France. Masson, Paris, pp. 249–334.
Brunet, M.-F., 1991. Subsidence et géodynamique du Bassin d'Aquitaine. Relations avec l'ouverture de l'Atlantique. Ph.D. Thesis, Université P. & M. Curie.
Carey, E., Brunier, B., 1974. Analyse théorique et numérique d'un modèle mécanique élémentaire appliqué à l'étude d'une population de failles. Comptes Rendus de l'Académie des Sciences 279 (D), 891–894.
Cavelier, C., Fries, C., Larrigues, J.L., Capdeville, J.P., 1997. Sédimentation progradante au Cénozoïque inférieur en Aquitaine méridionale: un modèle. Géologie de la France 4, 69–79.
Craddock, J.P., Jackson, M., Van Der Pluijm, B., Versical, R.T., 1993. Regional shortening fabrics in eastern north America: far-field stress transmission from the Appalachian–Ouachita orogenic belt. Tectonics 12, 257–264.
Debelmas, J., 1986. L'héritage hercynien à l'origine des grands bassins sédimentaires français. Bulletin des Centres de Recherche d'Exploration–Production Elf-Aquitaine 10, 151–161.
Deffontaines, B., 1990. Développement d'une méthodologie d'analyse morphostructurale et morphotectonique. Analyse des sufaces enveloppes, du réseau hydrographique, et modèles numériques de terrain. Applications au NE de la France. Ph.D. Thesis, Univ. P. & M. Curie, Rapport Interne BRGM 32005.
Deffontaines, B., Chorowicz, J., 1991. Principles of drainage basin analysis from multisource data: application to the structural analysis of the Zaire Basin. Tectonophysics 194, 237–263.
Déramond, J., Souquet, P., Fondecave, M.-J., Specht, M., 1993. Relationships between thrust tectonics and sequence stratigraphy surfaces in foredeeps: model and examples from the Pyrenees (Cretaceous–Eocene, France, Spain). Geological Society Special Publication 71, pp. 193–219.
Dietrich, D., Song, H., 1984. Calcite fabrics in a natural shear environment: the Helvetic nappes of western Switzerland. Journal of Structural Geology 6, 19–32.
ECORS Pyrenees team, 1988. The ECORS deep reflection seismic survey across the Pyrenees. Nature 331, 508–511.
Etchecopar, A., 1984. Etude des états de contraintes en tectonique cassante et simulation de déformations plastiques (approche mathématique). Ph.D. Thesis, Univ. Sciences & Techniques du Languedoc, Montpellier.
Etchecopar, A., Vasseur, G., Daignieres, M., 1981. An inverse problem in microtectonics for the determination of stress tensor from fault striation analysis. Journal of Structural Geology 3, 51–65.
Grellet, B., Combes, P., Granier, T., Philip, H., Mohammadiou, B., 1993. Sismotectonique de la France métropolitaine. Mémoires de la Société Géologique de France 164, 76 p.
Guimerà, J., 1984. Paleogene evolution of deformation in the northeast Iberia Peninsula. Geological Magazine 121, 413–420.
Guimerà, J., Alvaro, M., 1990. Structure de la compression alpine dans la Chaîne ibérique et la Chaîne côtière catalane (Espagne). Bulletin de la Société Géologique de France 8, 339–348.
Hervouët, Y., Klarica, S., Roddaz, B., 1997. Déformations alpines, inversion tectonique négative et karstogenèse: exemple de la Pierre Saint-Martin (Pyrénées-Atlantiques, France). Bulletin de la Société Géologique de France 168, 663–674.
Klitgord, K., Schouten, H., 1986. In: Vogt, P.R., Tucholke, B.E. (Eds.), Plate kinematics of the Central Atlantic. The Western North Atlantic Region: Boulder, Colorado. Geological Society of America, The Geology of North America M, pp. 351–377.
Lacombe, O., Angelier, J., Laurent, P., 1992. Determining paleostress orientations from faults and calcite twins: A case study near the Sainte-Victoire Range (southern France). Tectonophysics 201, 141–156.
Lacombe, O., Laurent, P., 1992. Determination of principal stress magnitudes using calcite twins and rock mechanics data. Tectonophysics 202, 83–93.
Lacombe, O., Laurent, P., Rocher, M., 1996. Magnitude de la contrainte déviatorique pyrénéenne dans l'avant-pays nord-pyrénéen. Comptes Rendus de l'Académie des Sciences Paris 322 (IIa), 229–235.
Laurent, P., 1984. Les macles de la calcite en tectonique: nouvelles méthodes dynamiques et premières applications. Ph.D. Thesis, Université des Sciences & Techniques du Languedoc, Montpellier.
Lefort, J.P., 1989. Basement correlation across the north Atlantic. Springer-Verlag, Berlin, 148 pp.
Le Pichon, X., Bergerat, F., Roulet, M.-J., 1988. Plate kinematics and tectonics leading to the Alpine belt formation; a new analysis. Geological Society of America, Special Paper 218, pp. 111–131.
Lepvrier, C., Mougenot, D., 1984. Déformations cassantes et champs de contraintes posthercyniens dans l'Ouest de l'Ibérie (Portugal). Revue de Géologie Dynamique et de Géographie Physique 25, 291–305.
Mathieu, C., 1986. Histoire géologique du sous-bassin de Parentis. Bulletin des Centres de Recherche d'Exploration–Production Elf-Aquitaine 10, 33–47.
Martin, R., 1992. La fracturation dans les domaines chevauchants et leurs avant-pays: comparaison entre le Wyoming (E.-U.) et le Béarn (France). Conséquences. Ph.D. Thesis, Université Toulouse III.
Pfiffner, O.A., Burkhard, M., 1987. Determination of paleostress axes orientations from fault, twin and earthquake data. Annales Tectonicae 1, 48–57.
Rocher, M., Lacombe, O., Angelier, J., Chen, R.W., 1996. Mechanical twin sets in calcite as markers of recent collisional events in a fold-and-thrust belt: evidence from the reefal limestones of southwestern Taiwan. Tectonics 15, 984–996.
Rocher, M., 1999. Déformations et paléocontraintes des avant-pays de chaînes de collision: les piedmonts occidentaux de Taïwan et le bassin Sud-aquitain. Ph.D. Thesis, Université P. & M. Curie, Paris.
Rowe, K.J., Rutter, E.H., 1990. Paleostress estimation using calcite twinning: experimental calibration and application to nature. Journal of Structural Geology 12, 1–17.
Scanvic, J.Y., 1983. Utilisation de la télédétection dans les Sciences de la Terre. Manuels et méthodes. Bureau de Recherche Géologique et Minière 7, 159 pp.
Solomon, S.C., Richardson, R.M., Bergman, E.A., 1980. Tectonic stresses: models and magnitudes. Journal of Geophysical Research 85 (B11), 6086–6092.
Stévaux, J., Zolnaï, G., 1975. Les olistostromes du sud de l'Aquitaine dans la dynamique du bassin. Tectonique et sédimentation 2, 9e Congrès interne Sédimentologie, Nice.
Sztràkos, K., Gély, J.-P., Blondeau, A., Muller, C., 1997. Le Paléocène et l'Ilerdien du Bassin sud-aquitain: lithostratigraphie, biostratigraphie et analyse séquentielle. Géologie de la France 4, 27–54.
Sztràkos, K., Gély, J.-P., Blondeau, A., Muller, C., 1998. L'Eocène du Bassin sud-aquitain: lithostratigraphie, biostratigraphie et analyse séquentielle. Géologie de la France 4, 57–105.
Thomas, G., Delfaud, J., 1990. Mise en évidence de décrochements dextres NW–SE contemporains de la sédimentation oligo-miocène dans le bassin de Jaca-Pampelune (Pyrénées sud-occidentales, Espagne). Comptes Rendus de l'Académie des Sciences Paris II, 801–806.
Tourneret, C., 1990. I: Maclage et états de contraintes dans les roches carbonatées du domaine fragile. Application à des plates-formes d'avant-pays de chaînes (Pyrénées, Alpes); II: Recherche des directions des contraintes tectoniques dans trois champs d'hydrocarbures d'Aquitaine. Ph.D. Thesis, Université de Montpellier II.
Tourneret, C., Laurent, P., 1990. Paleostress orientations from cal-

cite twins in the north Pyrenean foreland, determined by the Etchecopar inverse method. Tectonophysics 180, 287–302.

Tullis, T.E., 1980. The use of mechanical twinning in minerals as a measure of shear stress magnitudes. Journal of Geophysical Research 85, 6263–6268.

Turner, F.J., 1953. Nature and dynamic interpretation of deformation lamellae in calcite of three marbles. American Journal of Sciences 251, 276–298.

Turner, F.J., Griggs, D.T., Heard, H., 1954. Experimental deformation of calcite crystals. Geological Society of America Bulletin 65, 883–934.

Winnock, E., 1974. Debelmas, J. (Ed.), Géologie de la France, vol. 1, pp. 255–293.